Cryo-electron tomography of the herpesvirus procapsid reveals interactions of the portal with the scaffold and a shift on maturation

Michael H. C. Buch[a,$], William W. Newcomb[a,$], Dennis C. Winkler[a,b], Alasdair C. Steven[a,#], J. Bernard Heymann[a,#]

[a] Laboratory of Structural Biology Research, National Institute of Arthritis and Musculoskeletal and Skin Diseases, National Institutes of Health, Bethesda, MD, US.

[b] Advanced Imaging Core, National Institute on Deafness and Other Communication Disorders, National Institutes of Health, Bethesda, MD, US.

[$] These authors contributed equally to this study.

[#] Corresponding authors. Contact: heymannb@mail.nih.gov , stevena@mail.nih.gov

Running title: Visualizing the herpes portal in the procapsid

16 **Abstract**

17 Herpes simplex virus type 1 (HSV-1) requires seven proteins to package its genome through a
18 vertex in its capsid, one of which is the portal protein, pUL6. The portal protein is also thought to
19 facilitate assembly of the procapsid. While the portal has been visualized in mature capsids, we
20 aimed to elucidate its role in the assembly and maturation of procapsids using cryo-electron
21 tomography. We identified the portal vertex in individual procapsids, calculated a subtomogram
22 average, and compared that with the portal vertex in empty mature capsids (A-capsids). The
23 resulting maps show the portal on the interior surface with its narrower end facing outwards,
24 while maintaining close contact with the capsid shell. In the procapsid, the portal is embedded in
25 the underlying scaffold, suggesting that assembly involves a portal – scaffold complex. During
26 maturation, the capsid shell angularizes with a corresponding outward movement of the vertices.
27 We found that in A-capsids, the portal translocates further than the adjacent capsomers and
28 strengthens its contacts with the capsid shell. Our methodology also allowed us to determine the
29 number of portal vertices in each capsid, with most having one per capsid, but some none or two,
30 and rarely three. The predominance of a single portal per capsid supports facilitation of the
31 assembly of the procapsid.

32

33 **Importance**

34 Herpes simplex virus type 1 (HSV-1) infects a majority of humans, causing mostly mild disease
35 but in some cases progressing towards life-threatening encephalitis. Understanding the life cycle
36 of the virus is important to devise countermeasures. Production of the virion starts with the
37 assembly of an icosahedral procapsid including DNA packaging proteins at a vertex, one of which
38 is the dodecameric portal protein. The procapsid then undergoes maturation and DNA packaging
39 through the portal, driven by a terminase complex. We used cryo-electron tomography to
40 visualize the portal in procapsids and compare them to mature empty capsids. We found the
41 portal located inside one vertex interacting with the scaffold protein in the procapsid. On
42 maturation, the scaffold dissociates, the capsid angularizes, and the portal moves outward,
43 associating closely with the capsid shell. These transformations may provide a basis for the
44 development of drugs to prevent HSV-1 infections.

45
46 **Introduction**

47 Members of the *Herpesviridae* family cause persistent infections in humans, ranging from cold
48 sores on the lips and genitals to shingles and tumors. While individual members of this family
49 exhibit differences in pathogenicity and structural details, reflected in their classification into
50 three subfamilies, their overall architecture is largely conserved. The large genome of HSV-1, the
51 prototypical representative of *Herpesviridae*, is accommodated in a correspondingly massive and
52 complex capsid. During their elaborate life cycle (1), nascent capsids assemble in the nucleus as
53 spherical precursor particles called procapsids (2-4), which conform to T=16 quasi-icosahedral
54 symmetry and contain a spherical internal scaffold. The scaffold shell consists of the viral proteins
55 pUL26.5 and pUL26, of which the latter has an N-terminally module, the viral protease (4). Upon
56 completion of the procapsid, the protease is activated and proceeds to cleave the scaffold,
57 initiating maturation of the capsid. Maturation involves: (I) angularization of the capsid; (II)
58 reorganization of the interactions that engage the triplex proteins as well as rearrangement of
59 capsomers (1-3) from skew to more symmetric orientations; (III) conformational changes (2, 5-8)
60 that establish interactions between capsomer subunits; and (IV) decoration of the mature capsid
61 with additional proteins (9, 10). Maturation increases the capsid's stability dramatically,
62 countering the internal pressure exerted by the tightly packed genome (11). This process yields
63 three capsid species, two of which remain in the nucleus. The A-capsid has a mature shell that
64 does not contain any DNA and is essentially empty, while B-capsids retain a shrunken and
65 somewhat disordered scaffold despite having matured into an angular shape. Only mature, DNA-
66 filled capsids, called C-capsids, leave the nucleus and do so via the perinuclear space (reviewed
67 in (12, 13)), to undergo the subsequent steps in the viral life cycle.
68
69 DNA packaging occurs at a capsid vertex and requires seven proteins, pUL6, pUL15, pUL17,
70 pUL25, pUL28, pUL32 and pUL33 (14). pUL6 forms a circular dodecamer similar to the portals of
71 bacteriophages (15) and may facilitate procapsid assembly (16). Heterotrimers of pUL17 (one
72 copy) and pUL25 (two copies) are bound to the pentons and peripentonal triplexes (17-19). A
73 terminase complex composed of pUL15, pUL28 and pUL33 provides the force for packaging and
74 subsequent cleavage of the DNA (20-26). The final protein, pUL32, has not been found as a

75 component of capsids (14). These proteins replace a penton presumably at one vertex of the
76 capsid (27). While the structural disposition and transformations of some of these components
77 have been elucidated, many details of assembly, maturation and packaging remain to be
78 described.
79
80 Early attempts to locate the portal-bearing vertex in capsids employed cryo-electron tomography
81 (cryoET) (28, 29). The tomograms were of low resolution (55-60 Å), complicating analysis. This
82 led to placing the portal either at the level of capsomers (28) or inside the capsid shell (29).
83 Subsequent analysis employing cryo-electron microscopy (cryoEM) and single particle analysis
84 (SPA), indicated that the portal is located inside the capsid shell (30, 31). One of the difficulties in
85 the SPA approach is that the overlap of one vertex with the large mass of the capsid (~100 fold
86 ratio) makes it hard to distinguish a portal vertex from the penton vertices. Nevertheless, the
87 extensive averaging of structural information means that correct assignments would dominate
88 incorrect assignments distributed over the eleven other possibilities and reveal the location of
89 the portal. The recent technological advances in cryoEM enabled the high resolution
90 reconstruction of various herpesvirus capsids showing the portal on the inside of one vertex (18,
91 31-34).
92
93 One omission from the existing studies is the predisposition of the portal in the initial assembly
94 product, the procapsid. It is also not clear that only one vertex bears a portal as assembly can
95 occur without portal (2). In this study, we returned to cryoET to examine the portal vertices in
96 procapsids and compared them to A-capsids as a control. In this effort, we developed the
97 computational capability to find the portal vertices in a more reliable manner, allowing an
98 estimate of the number of portal vertices in each capsid. From subtomogram averages of the
99 portal vertices, we found abundant contacts between the portal and the scaffolding layer in the
100 procapsid. We also found that the portal moves closer to the capsid shell on maturation.
101

102 **Results**

103

104 **Production of procapsids.** Procapsids were produced using the M100 mutant that lacks the viral
105 protease VP24 required for rapid maturation (35). We followed a gentle purification protocol (5,
106 7) to minimize damage to the particles. For successful identification of the portal vertex in
107 procapsids, several precautions were taken: since procapsids are fragile and malleable, we used
108 an antibody binding to the major capsid protein (2) that stabilized the particles. We performed
109 cryoET on the isolated procapsids, collecting and analyzing 80 tilt series where the particles were
110 well separated (Fig. 1A).

111

112 **Production of capsid samples using a pUL25-deficient mutant.** We decided to analyze mature
113 A-capsids as a control to avoid interference from internal density features such as scaffolding (cf.
114 B-capsids) or packaged DNA (cf. C-capsids). The established protocol for purifying HSV-1
115 nucleocapsids from a wild-type infection yields only a minor fraction of A-capsids. To increase
116 their yield, we used a mutant lacking the vertex protein, pUL25, that is defective in DNA packaging
117 (36). This virus replicates in a complementary African Green Monkey cell line transfected with
118 the *UL25* gene, but in wild-type cells cannot produce progeny. In our protocol, centrifugation on
119 small-scale sucrose gradients yielded bands for A-capsids and B-capsids but no band for the DNA-
120 filled C-capsids (Fig. 1C). We isolated the UL25-Null A-capsid band (hereafter referred to as A-
121 capsids) and collected tilt series for cryoET. Individual capsids in the tomograms were well spread
122 out in the sample, and almost all capsids could be confirmed as A-capsids from their empty
123 appearance (Fig. 1B).

124

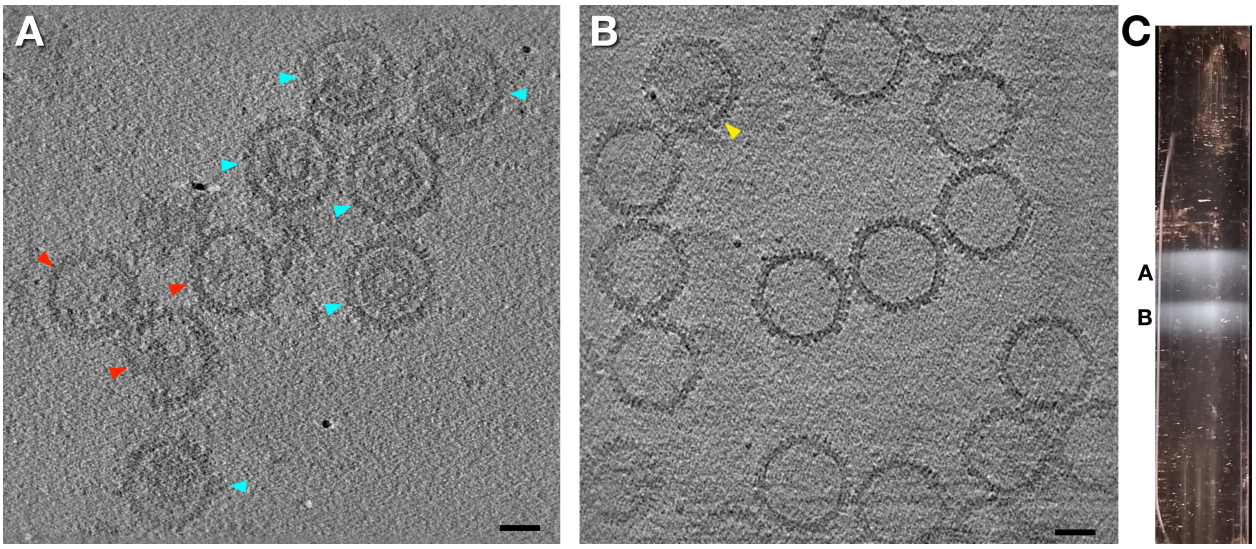

Fig. 1. Isolated capsids. A. Central slice of a tomogram of procapsids. Some particles contained visibly degraded scaffold or showed imperfections (red arrowheads) and were excluded from further processing. We took care to include only particles that were separated, spherical, and had a visibly intact scaffold (turquoise arrowheads). **B.** Central slice of a tomogram of A-capsids. The individual particles are well defined and separated. Occasionally, a capsid with some internal content – probably some scaffold – were found in the field of view (yellow arrowhead). These particles were not included in further processing. **C.** Small-scale sucrose gradient of a capsid mix obtained during initial purification from a UL25-Null mutant, showing bands of A- and B-capsids. Scale bars, 500 Å.

Identification of the portal vertex in cryo-electron tomograms. Our aim was to locate the portal using cryoET to take advantage of the straightforward identification of unique features in 3D maps. The approach used in an earlier tomographic protocol relied on simple template matching to find the portal vertex (28). Another protocol made use of the comparison of opposite vertices and assessing the density differences between vertices (30). In an effort to improve the detection of portal vertices, we developed a different algorithm aimed at detecting the vertex that is most different from the other vertices. We implemented this algorithm in a new program called bico added to the existing Bsoft package (37). An overview of our workflow is given in Fig. 2. From reconstructed tomograms, subtomogram volumes were extracted and aligned to an icosahedral reference, in our case a reconstruction of a HSV-1 C-capsid (accession number EMDB-7472 (38)).

146 Next, the fivefold vertices of each capsid were extracted, and an average of all extracted and
147 correctly oriented vertices was calculated. To focus only on the central part of a vertex where we
148 expect the biggest difference between penton and portal, we used a soft cylindrical mask in the
149 comparisons of each vertex with the average (see Materials and Methods for mask details). For
150 each set of 12 vertices, bico then classified each vertex set into two subsets: the first subset
151 contained the eleven best-fitting vertices. The second subset contained the vertex with the worst
152 fit, taken to be the portal vertex. The coordinates of the identified portal vertices were then
153 transferred back into the extracted and aligned capsids, and a reconstruction of the capsid
154 featuring the portal vertex was calculated. To reduce noise, this reconstruction was symmetrized
155 fivefold in the final step and filtered to 30 Å (just beyond the 34 Å resolution estimated by Fourier
156 shell correlation – see Fig. S1).
157

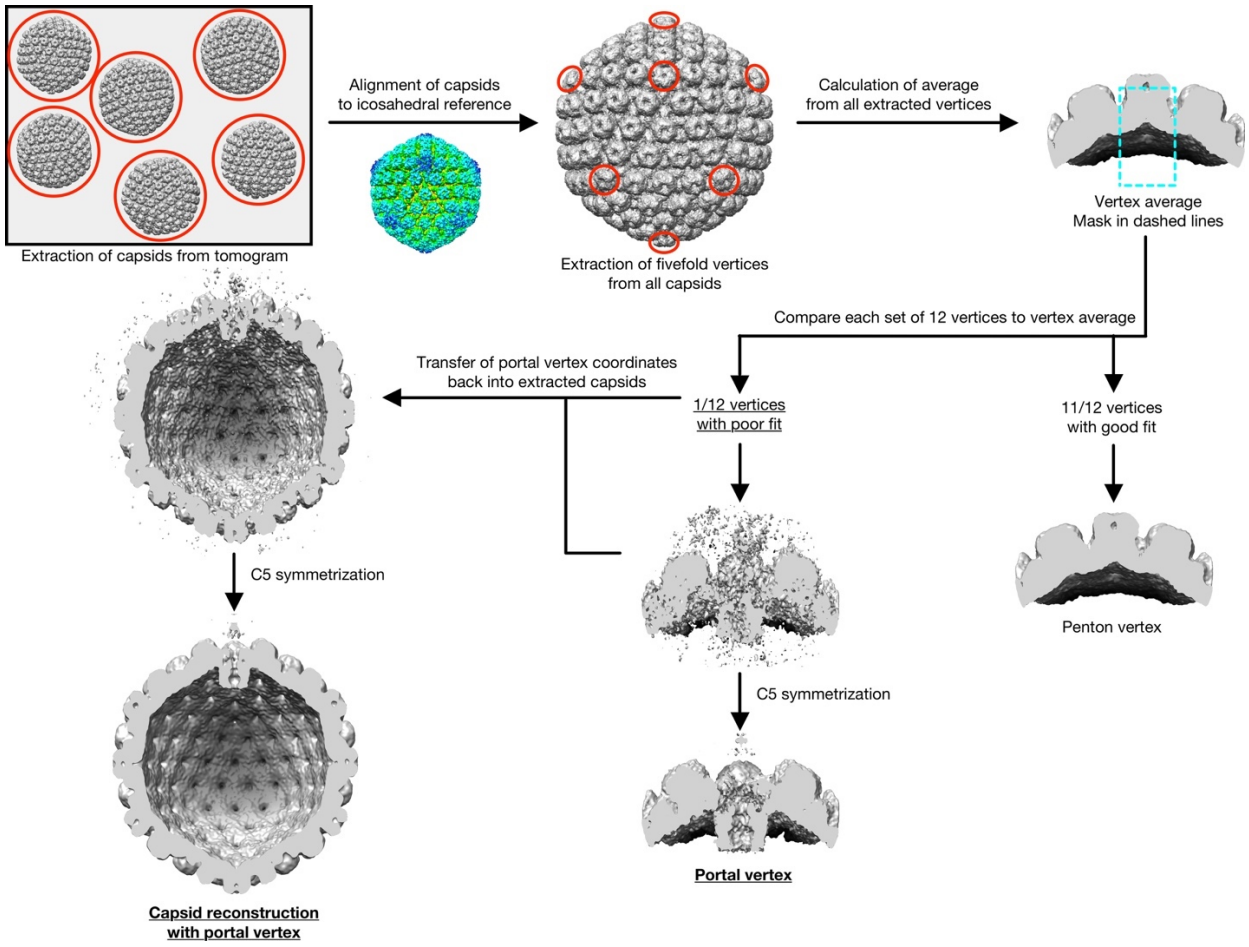

158

159 **Fig. 2.** Workflow used to identify and average the portal vertices. Individual particles (volumes
160 each containing a capsid) extracted from tomograms and aligned with an icosahedral reference
161 using a frequency space mask to compensate for the missing wedge. This allows the location of
162 the twelve 5-fold vertices of each capsid, which are then extracted and averaged. Each vertex is
163 correlated to this average using a missing wedge mask in frequency space and a cylindrical real
164 space soft mask to isolate the region in a vertex occupied by the penton or portal (cyan dashed
165 line). The vertex with the lowest (worst) correlation is assumed to contain the portal. This is
166 followed by a further refinement to find the best 5-fold orientation around the vertex axis. The
167 coordinates of the portal vertices were then used to transform their corresponding capsids into
168 orientations that placed the portal vertex on the z-axis at the top of the volume.
169
170
171 **The portal-bearing vertex of UL25-Null A-capsids.** We extracted a total of 164 subtomogram
172 volumes of A-capsids from our tomograms. We identified the likely portal-bearing vertex in the
173 map of each of the A-capsids and calculated an average (Fig. 3), obtaining a resolution of 34 Å
174 (Fig. S1). In line with recent publications (18, 32, 33), we visualized the portal on the inside of the
175 capsid, with its wider end facing towards the center of the particle (Fig. 3A). A superposed atomic
176 model of the HSV-1 portal (PBD ID 6OD7 (32)) fits well into the portal density (Fig. 3B). The portal
177 has a narrow end called the "clip domain" that engages the triplexes (green arrow in Fig. 3B) (for
178 the assignment of this density as a triplex, see Huet et al. (31)). The widest part of the portal, the
179 "wing domain" extends towards the floors of the neighboring capsomers (blue arrow in Fig. 3B).
180 The overall appearance and placement of this connection is consistent with a set of β-barrels and
181 spine helices originating from the pUL19 hexons that were identified earlier in a high-resolution
182 reconstruction (32). Knowing what it looks like, we could identify the portal vertex in individual
183 particles in our tomograms (white arrows in Fig. 3C).
184

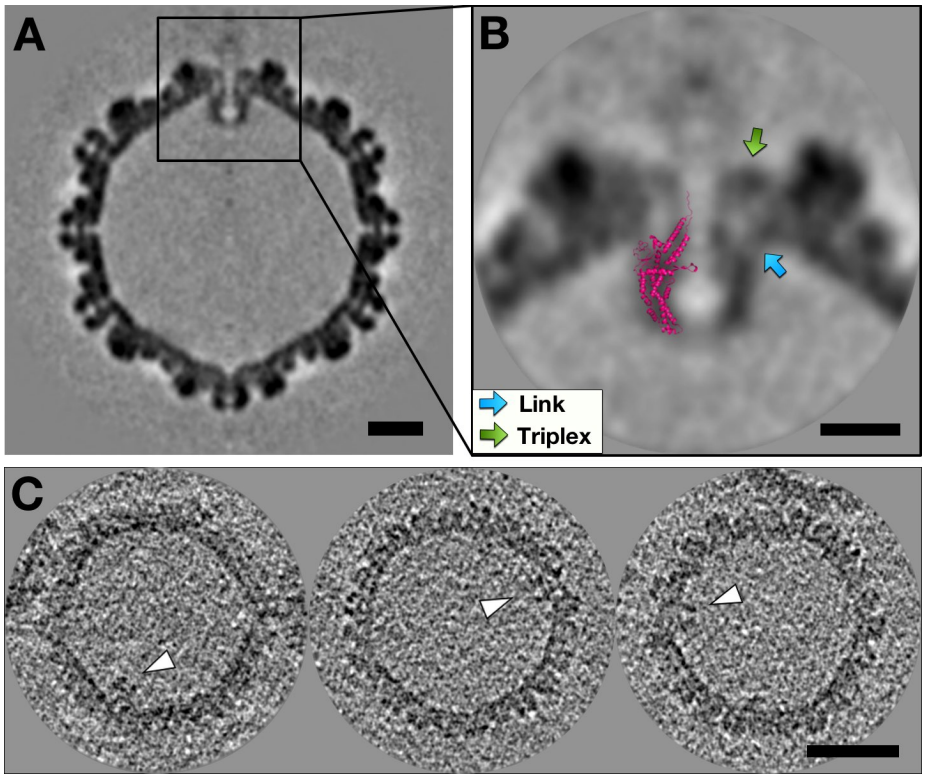

Fig. 3. The portal vertex in UL25-Null A-capsids. A. Central slice of the C5-symmetrized capsid with the portal vertex located at the top. Scale bar, 200 Å. **B.** Magnified view of the vertex. The portal is located beneath the capsid floor with its wider end facing the inside of the particle. A high-resolution model (pink, PDB ID 6OD7 (32)) is superimposed on the left half of the portal density. The portal forms connections to the triplex (green arrow) and the capsid floor (blue arrow indicates a link). Note that there is a diffuse density above the portal vertex that could be residual terminase. Scale bar, 100 Å. **C.** Slices from tomograms of A-capsids that traverse the portal in each (white arrowheads). Scale bar, 500 Å.

The portal in procapsids interacts with the scaffold. We selected tomograms with well-separated spherical particles (Fig. 1A) and extracted 368 subvolumes. As with A-capsids, we identified the portal-bearing vertex, taking care to adjust the mask so that it excluded the scaffold, which might otherwise outweigh the portal density during vertex sorting. After identifying the portal vertex in each procapsid, we calculated an average (Fig. 4) with a resolution of 34 Å (Fig. S1). Consistent with the A-capsids, the portal is located inside the capsid shell (Fig.

202 4A), and again agrees with an atomic portal model (Fig. 4B). The portal penetrates deeply into
203 the scaffold layer (yellow arrow in Fig. 4B), almost to the widest part of its wing, a position that
204 allows the formation of extensive interactions. Interestingly, the nominally spherical scaffold
205 shows a degree of perturbation caused by the portal, giving the scaffold an overall teardrop
206 shape (Fig. 4A). We also note that – apart from in the portal region - the scaffold shell shows up
207 in slices as three concentric shells (arrows in Fig. 4A) consistent with previous studies (5, 7). Only
208 tenuous contacts (blue arrow in Fig. 4B) are formed between the portal wing domain and the
209 surrounding hexons, but the clip domain appears to interact with the triplexes (green arrow in
210 Fig. 4B). The vertex overall has a funnel-like shape that likely accommodates DNA insertion by
211 the terminase complex. Finally, the procapsid hexons also display faint residual density on their
212 exterior parts that we attribute to the 6F10 antibody used to stabilize the procapsids during
213 isolation (Fig. 4A, 5C).
214
215

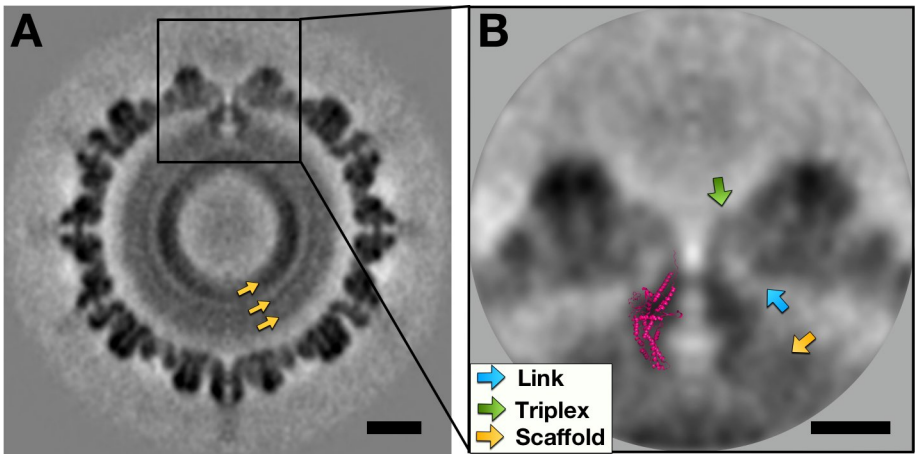

216
217 **Fig. 4. The portal vertex in procapsids. A.** Central slice of the C5-symmetrized procapsid with
218 the portal vertex at the top, showing distinct rings of scaffold density (yellow arrows). Scale bar,
219 200 Å. **B.** Magnified view of the portal vertex with a superimposed atomic model (pink, PDB ID
220 6OD7 (32)). The portal is mainly connected to the capsid through the triplex (green arrow) with
221 a thin connection to the capsid floor (blue arrow). The bottom of the portal is embedded in the
222 scaffold (yellow arrow). Scale bar, 100 Å.
223

224

225 **Conformational changes and movement of the portal during maturation.** While the portal
226 orientation is similar in procapsids and A-capsids, contrasts in vertex configuration come to light
227 in a side-by-side comparison (Fig. 5). Upon maturation, the capsid becomes angular, causing all
228 the vertices (both penton and portal) to translocate outwards. We assessed the movement of
229 the pentons by shifting the penton vertex of the procapsid outwards until it overlays the A capsid
230 penton, yielding a translation of 29 Å. Similarly, we measured the translation of the portal to be
231 54 Å, thus moving closer to the capsid shell. The portal in Fig. 5A appears to be somewhat
232 separated from the capsid shell but is much closer in the mature capsid (Fig. 5B). During
233 maturation, the capsid shell stabilizes by closure of the floor and burying interfaces between the
234 capsomers (8). Our results indicate that the portal also adopts a more stable interaction with the
235 mature capsid shell.

236

237 In addition, we observe a shift in the triplex network surrounding the portal vertex, which
238 narrows the vertex channel. These changes become even more apparent when the vertices are
239 viewed from the top (Fig. 5C,D). While triplexes are somewhat weakly defined in the procapsid
240 portal vertex, they become much more visible in the A-capsid and even extend towards the
241 fivefold symmetry axis. It is possible that some of this extending density could be ascribed to
242 components of the tegument, particularly pUL17. We recall that, upon maturation, the hexons
243 rearrange from a skewed orientation to true hexameric symmetry (8).

244

245 We also compared the triplexes of the portal vertex with those of the opposing penton vertex in
246 both maps. The triplexes in the procapsid portal vertex are poorly defined (Fig. 6A), making it
247 hard to ascertain whether they are in the same conformation as those at the opposing penton
248 vertex (Fig. 6B). In contrast, the orientations of the triplexes in the A-capsid are clearly the same
249 for both vertices (Fig. 6C,D).

250

251

252

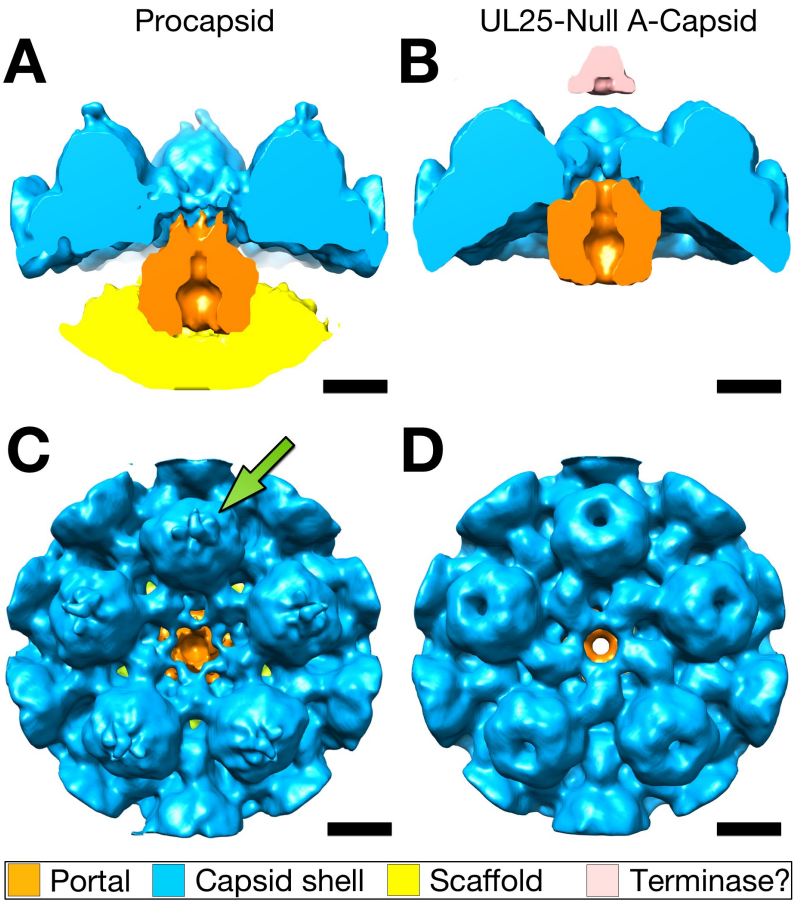

Fig. 5. Comparison of portal vertices in procapsid and UL25-Null A-capsid. A. Side view cut through the procapsid portal vertex, showing the portal (orange) connecting to the capsid shell (blue) and embedded in the scaffold (yellow). **B.** Side view of the mature A-capsid portal vertex, with the portal (orange) very closely associated with the capsid shell (blue). The diffuse density above the vertex (pink) may be residual terminase. **C.** Top view of the procapsid portal vertex with faint density associated with the tops of the hexons attributed to the 6F10 antibody used in the preparation of the particles (green arrow). **D.** Top view of the A-capsid portal vertex. Upon maturation, the triplexes surrounding the vertex shift and constrict the vertex channel, and the hexons transform from skewed ovals towards hexagonal symmetry. Scale bars, 100 Å.

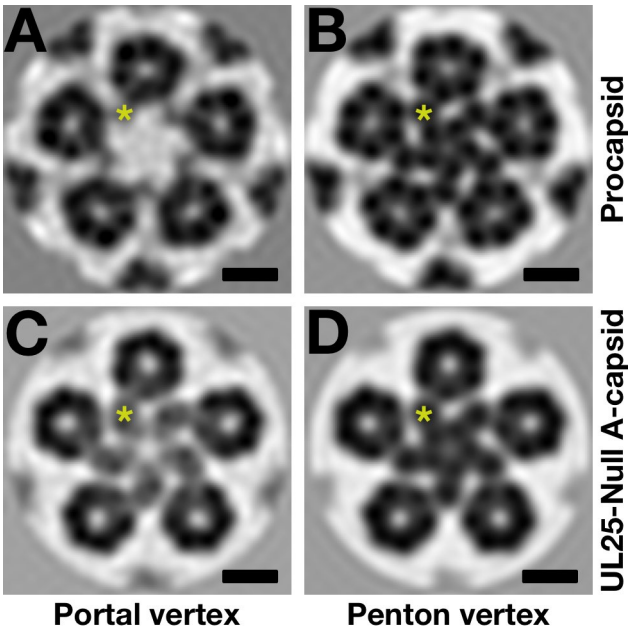

Fig. 6. The arrangement of triplexes at the vertices. The triplexes (yellow stars) at the procapsid portal vertex (**A**) are recessed relative to those at the opposite penton vertex (**B**) (slices at a radius of 307 Å). In contrast, the triplexes at the A-capsid portal vertex (**C**) are closer in conformation to those at the opposite penton vertex (**D**) (slices at a radius of 325 Å). Note that the vertices in the procapsid move outwards by ~29 Å on maturation, accounting for the differences in slices shown here. Scale bars, 100 Å.

The number of portal vertices per capsid. While we implicitly assumed there is exactly one portal per capsid, that is not necessarily true. To determine the number of portal vertices in each capsid, we examined the distribution of correlation coefficients for the 12 vertices. Our aim was to generate two clusters: the few with the worst correlation coefficients indicating portal vertices, and the rest as penton vertices. To separate the clusters, we took the biggest difference between successive correlation coefficients in a sorted list as the distinction between penton and portal vertices. Because we expected only a few portal vertices, only the six with the lowest coefficients were assessed. However, this strategy assumes there is at least one portal vertex. We compared the difference between the two worst vertices with the next three differences and assumed that when it is the lowest, it indicated a capsid without a portal vertex. The resultant distributions are shown in Fig. 7, giving average portal vertices per capsid

283 of 1.07 for procapsids and 1.25 for A-capsids, consistent with previous estimations (16, 27). In
284 our subtomogram averages, we included all of the capsids, but we do not consider the minor
285 contribution of the capsids without portals to significantly change our conclusions. About 65 %
286 of the capsids have a single portal vertex, in agreement with the 73 % reported for A-capsids
287 (28). A still significant number (~20 %) have two portal vertices, while those with three are rare.
288 If the incorporation of portal vertices follows a random pattern, the expected distribution
289 would be binomial in nature (blue lines in Fig. 7). The predominance of a singly incorporated
290 portal indicates that the assembly is more specific than a random process.
291

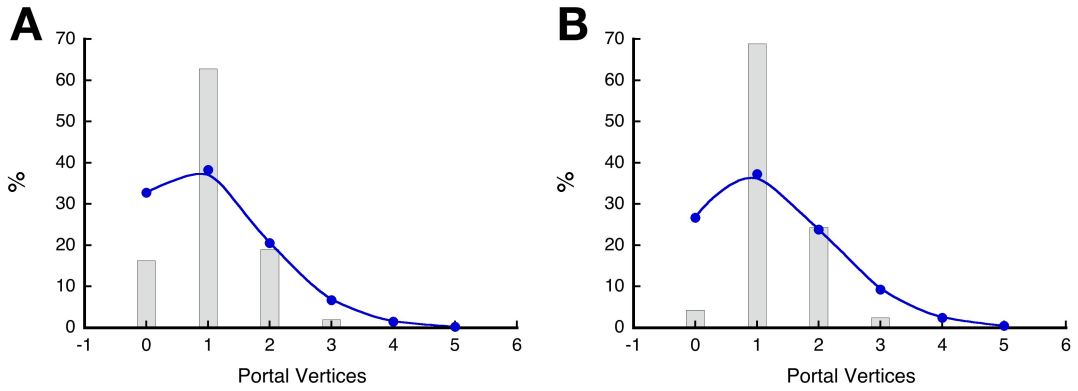

292
293 **Fig. 7.** Estimating the number of portal vertices (bars) per procapsid (A) an A-capsid (B). The
294 blue line in each plot is a binomial distribution calculated from the average number of portal
295 vertices per capsid as an indication of expected random incorporation.
296
297
298 **Discussion**
299 **Localization and interactions of the portal in procapsids compared to A-capsids.** In a critical step
300 of the HSV-1 life cycle, newly synthesized DNA is threaded into the capsid which undergoes
301 extensive conformational changes as it matures (5, 8) although the latter process can occur
302 without DNA packaging (8) and may precede DNA packaging *in vivo* (39). In both herpesviruses
303 and tailed bacteriophages, DNA is inserted through a fivefold vertex via the dodecameric portal
304 protein and driven by terminase complex. While the overall structure of the HSV-1 portal, pUL6,
305 has been known for some time (15), its orientation and placement in the context of the capsid

306 shell have been subject to debate. The portal's overall shape makes it difficult to distinguish
307 visually from capsomer pentons in micrographs, making consistent alignment of 2D projections
308 a challenge. In an earlier study, we used cryoET, aiming to characterize the portal vertex of HSV-
309 1 (28). Here, we have refined this approach by developing a new program designed to identify
310 the portal vertex on individual capsids, thereby allowing coherent averaging. Applying it to HSV-
311 1 procapsids and A-capsids, we located the portal on the inside of the particle, consistent with
312 several recent SPA-based studies (18, 30, 32-34). In confirmation, an atomic model of pUL6 (32)
313 fits well into our portal density (Fig. 8). This density extends beyond the clip domain of the model,
314 presumably representing some of residues 308-515, which were not modeled (corresponding
315 residues are also unmodeled in a reconstruction of the Epstein-Barr-virus portal (40)).
316 Interestingly, a corresponding turret-shaped density was discovered in the portal vertex of
317 Kaposi's Sarcoma Herpesvirus (KSHV) (34); it was theorized that this helical turret is an extension
318 of the portal's clip domain and could be a docking site for the terminase complex. If such a
319 component is indeed an additional protein, it may only be added to mature particles upon the
320 successful retention of DNA.
321

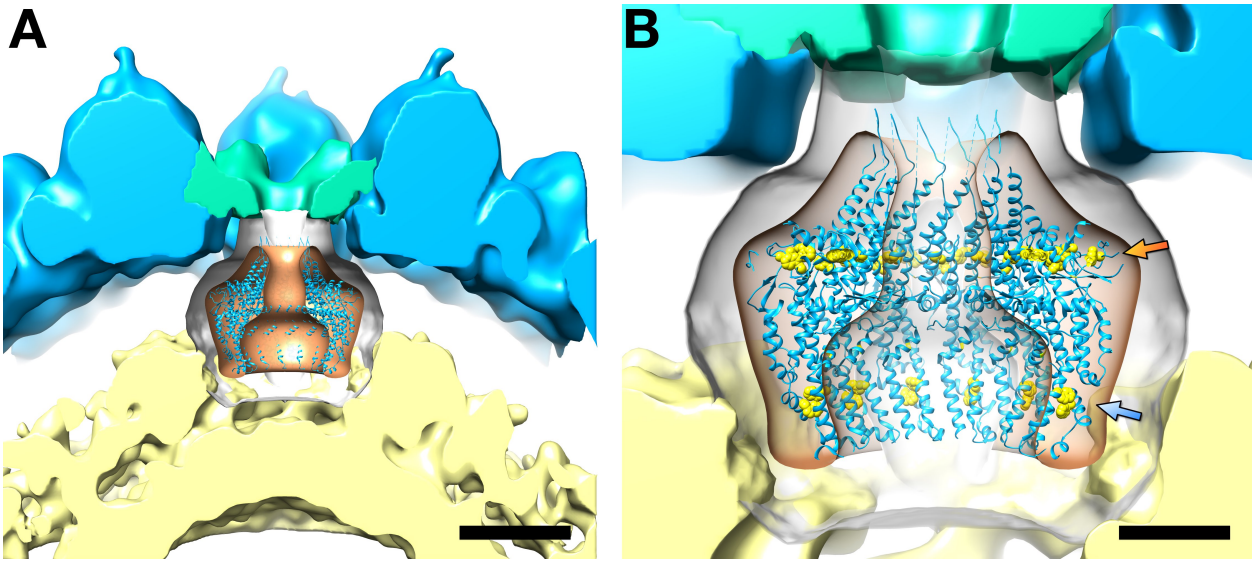

322
323 **Fig 8**. **The model of the portal within the context of the procapsid portal vertex. A.** The portal
324 model (PDB ID 6OD7 (32)) fitted into the portal density (orange) within a lower threshold
325 envelope (grey) to show the connections to the triplexes around the portal (green) and the
326 scaffold (yellow). The connections to the capsid shell (composed of the major capsid protein

327 and other triplexes shown in blue) are not resolved in this map. Scale bar, 100 Å. **B.** Close-up
328 view of the portal with key tryptophan residues (yellow balls) at the wing (orange arrow: W163,
329 W241, W262, W532) and at the bottom (blue arrow: W90, W127) that were shown to interact
330 with the scaffold (41). Scale bar, 40 Å.
331
332 Applying our workflow to procapsids led to several novel observations. The procapsid portal is
333 located inside the vertex forming contacts with the scaffolding shell and deforming the scaffold
334 proteins' spherical arrangement at the interaction site. Conserved tryptophan residues have
335 been identified in HSV-1 pUL6 ((41), see also Fig. 2 in (42)) that play crucial roles in interaction
336 between portal and, most likely, conserved scaffold residues 143-151 of pUL26, particularly
337 YYPGE (43, 44). Figure 8B shows these critical tryptophan residues arrange in a ring in the wing
338 domain (orange arrow in Fig. 8B) as well as a ring in the base of the portal (blue arrow in Fig. 8B).
339 We know the scaffold C-terminus is bound to the capsid (45) which puts it in the proximity of the
340 portal wing domain. Conserved tryptophan residues are a feature not only of HSV-1 but also of
341 some bacteriophages ((46), reviewed in (42)). The scaffold probably shares the symmetry of the
342 surface shell with which it co-assembles but is not highly ordered and its apparent sphericity is
343 enhanced by averaging. From previous studies we know that the protease at the N-terminal part
344 of about 10 % of the scaffold proteins is located towards the center of the procapsid (4) and the
345 C-terminus interacts with the capsid shell (47) and portal (43). This means the protein is in an
346 extended radial conformation consistent with a side-by-side packing of coiled coil dimers as
347 inferred by Pelletier et al. (48). In the procapsid we see three peaks in the concentric density
348 shells (Fig. 4) in agreement with the three domains proposed by Trus et al. (7).
349
350 **Incorporation of the portal during procapsid assembly.** The stage at which the portal is
351 incorporated into the procapsid is still unknown, with possibilities that it could initiate assembly,
352 inserted at some intermediate point, or at the end (16). Procapsids can assemble *in vitro* without
353 portal present (2, 3) and some of the capsids we analyzed appear to lack a portal vertex (Figure
354 7). We also found an average copy number slightly larger than one and consistent with previous
355 studies (16, 27). If one assumes a random model of incorporation, it is expected to follow a

356 binomial distribution. However, Figure 7 shows it clearly deviates from a binomial pattern,
357 suggesting a predisposition towards a single portal vertex per capsid. This suggests that the portal
358 may facilitate procapsid assembly and thus ensure that a majority has at least one portal vertex.
359 However, if it initiates assembly, it does not preclude incorporation of one or two additional
360 portals.
361
362 **Morphological changes upon capsid maturation.** Cleavage of the C-terminal 25 residues of the
363 scaffolding protein by the protease (47) triggers maturation of the capsid shell. Our preparation
364 of procapsids is defective in the protease to allow us to purify it. Nevertheless, the capsids are
365 still able to mature slowly (8). On cleavage, the scaffold changes from extended in the procapsid
366 (i.e., large core particles) to somewhat contracted in the B-capsid (i.e., small core particles). At
367 the same time, the vertices of the capsid shell shift outwards during angularization by ~29 Å, with
368 the portal itself moving even further by ~54 Å (note that the capsid shells in A- and B-capsids are
369 very similar (31)). The portal therefore disengages from the scaffold to some extent, while
370 strengthening interactions with the capsid shell. The portal movement is accompanied by the
371 establishment of a support network with the newly established capsid floor (termed suspension
372 network in another study (32)).
373
374 The overall shape of the portal vertex differs significantly between procapsids and mature capsids
375 (Fig. 6). In procapsids, we note that the center of the vertex is essentially open, which would, in
376 a biological context, be advantageous for the insertion of DNA. Triplex density is present around
377 the portal vertex, but it is somewhat fainter than around a penton vertex, which could result
378 from a lack of interaction between the portal and the procapsid itself. In the mature capsid, the
379 vertex is narrower, and it appears that density originating at the triplexes extends towards the
380 vertex axis. This extended density may indeed be contributed by components of the tegument,
381 particularly pUL17. While our A-capsids lack pUL25, it has been shown that procapsids contain
382 practically no pUL25 (25), and given that the procapsid undergoes substantial conformational
383 changes during maturation, it is likely that no tegument component protein is present on these
384 immature particles. The extended, star-shaped density we see on the A-capsid portal vertex

385 (Fig. 5D) may therefore act as a docking platform for copies of pUL25 that would be added in the
386 course of a wild type infection and α-helices contributed by pUL36 at a later stage. This platform,
387 however, is evidently insufficient to retain DNA in the capsid, as the absence of pUL25 alone is
388 enough to completely prevent the emergence of propagation-competent, DNA-filled C-capsids
389 (36), underscoring pUL25's functional versatility as a DNA retention protein and a key player in
390 nuclear egress as well (49).
391
392 **Conclusion.** Our routine for processing cryo-electron tomograms enabled us to visualize the
393 portal in procapsids in comparison with mature A-capsids. Particularly revealing is the
394 interactions of scaffold with the portal likely to be involved in procapsid assembly. Quantitation
395 of the number of portal vertices per capsid further solidifies a role in assembly. We also gained
396 insight into the intricate maturation-induced changes in the portal vertex, visualizing an outward
397 movement of the portal exceeding vertex movement and thus stabilizing the interaction with the
398 capsid shell.
399
400 **Material and Methods**
401 **Cell handling and propagation of virus stocks.** Stocks of the UL25 deletion mutant (UL25-null)
402 (36) were generated by using a complementary African Green Monkey cell line (both gifts from
403 Prof. Fred L. Homa, University of Pittsburgh, Pittsburgh, PA). At roughly 75% confluency,
404 monolayers in 175 cm^2 flasks were infected with virus stock at a MOI of 0.1 in 1 mL of PBS without
405 calcium or magnesium per flask for 40 min at room temperature, followed by 5 min at 37˚C. The
406 cells were then overlaid with 15 mL virus growth medium (1x MEM Alpha, Corning, 1.5% (*v/v*)
407 penicillin/streptomycin) and incubated at 37˚C. At 48 h post infection, virus-containing medium
408 was clarified by centrifugation at 1,500 rpm for 5 min, and crude cell debris was removed from
409 the supernatant by pelleting at 6,000 rpm for 15 min in a Beckman SW28 rotor. Virus was pelleted
410 for 45 min at 19,000 rpm in a Beckman SW28 rotor. The virus pellets were resuspended in small
411 volumes of PBS without calcium or magnesium, and aliquots of 500 µL were frozen at -80˚C. The
412 virus titer was assessed in complementary cells 48 hr. after infection.

413 Stocks of the procapsid-producing M100 line (35) were generated similarly using the
414 complementary F-3 cell line. Stock titers were assessed as described earlier (5).
415 **Production of capsids.** Roller bottles of African Green Monkey cells were grown to about 75%
416 confluency and infected with UL25-null virus stocks at a MOI of 10. 14 hr post infection, cells had
417 started to round up, but not detach from the surface. Cells were harvested by centrifugation at
418 1,500 rpm for 5 min, and any virus still attached to the cell surface was removed by incubation
419 with TNE (20 mM Tris, pH 7.4, 500 mM NaCl, 1 mM EDTA) on ice for 15 min. Cells were again
420 pelleted for 5 min at 2,000 rpm, resuspended in TNE, and broken up by sonication. 1.5% (*v/v*)
421 TX-100 was added to solubilize nuclear membranes, followed by pelleting of crude cell debris for
422 30 min at 6,000 rpm in a Beckman SW28 rotor. The resulting supernatant was supplemented with
423 a cushion of 30% (*w/v*) sucrose in TNE, and a mix of A- and B-capsids was pelleted for 1 h at
424 20,000 rpm in a Beckman SW28 rotor. The pellets were resuspended in TNE, supplemented with
425 complete protease inhibitor cocktail (Roche), and applied to a preparative gradient containing a
426 range of 20-50% (*w/v*) sucrose in TNE. The gradient was run for 1 h at 22,000 rpm in a Beckman
427 SW55Ti rotor. Distinct bands containing the different capsid species were isolated, pelleted for
428 50 min at 22,000 rpm in a Beckman SW55Ti rotor, and resuspended in small amounts of TNE to
429 reach an appropriate concentration for cryoET.
430 Procapsids of the M100 mutant in the viral protease were produced as described earlier (5). They
431 were precipitated with the 6F10 antibody (raised against the triplex protein pUL19) for
432 purification and capsid stability purposes (4).
433 **Grid preparation and cryo-electron tomography.** Purified capsids were mixed with Aurion
434 Anionic 10 nm BSA gold tracers (EMS) at a 1:1 ratio, and 3 µL were applied to Quantifoil copper
435 grids covered with 300-mesh holey carbon (EMS), which were previously plasma-cleaned for 12
436 s with an argon-oxygen mixture (25% oxygen) in a Model 1020 plasma cleaner (Fischione, Export,
437 PA). Using a Leica EM GP plunger (Leica Microsystems, Buffalo Grove, IL), excess liquid was
438 blotted off for 2.5 s, and grids were flash-frozen in liquid ethane. For the A-capsids, 21 tilt series
439 ranging from -57˚ to +57˚ at 3˚ increments were collected at 20,000x magnification and a defocus
440 target of -2.5 µm on a JEOL JEM-2200FS cryo-electron microscope (JEOL USA, Peabody, MA)
441 operating at 200 kV and equipped with an in-column energy filter and a K2 Summit detector

442 (Gatan, Warrendale, PA). For procapsids, 80 tilt series ranging from -57˚ to +57˚ at 3˚ increments
443 at 81,000x magnification and a -2 µm defocus target were acquired on a 300 kV Titan Krios
444 (Thermo Fisher Scientific, FEI, Hillsboro, OR) equipped with a post-column Model 967 GIF
445 Quantum-LS with a K2 Summit detector (Gatan, Warrendale, PA). In both cases, data were
446 acquired using SerialEM (50).
447 **Tomogram reconstruction and identification of the portal-bearing vertex.** Image processing and
448 tomogram reconstruction were carried out using Bsoft (50, 51). Tomograms were binned 2-fold,
449 resulting in a final pixel size of 3.66 Å for A-capsids and 3.61 Å for procapsids. For both capsids,
450 promising particles were extracted in 450 x 450 x 450 pixel boxes (program bpick) and aligned
451 (program bfind) to a reference of a HSV-1 C-capsid (38) and using an appropriate frequency space
452 mask to compensate for the missing wedge (created with program bmissing). Given the correct
453 alignment parameters, the program bpick was used to extract the 12 vertices for each capsid
454 (150 x 150 x 150 pixel boxes) offset 140 pixels outward from the center of the particle on the
455 fivefold symmetry axes. Using the new Bsoft program, bico, for each set of 12 vertices was cross-
456 correlation against an average calculated from all vertices, and the vertex with the lowest
457 correlation was deemed the portal-bearing vertex. As for the whole capsid alignment, a
458 frequency space mask was used in the correlation calculation (created with program bmissing).
459 In addition, a real space mask was used to isolate a cylindrical region occupied by the penton at
460 the vertex. The mask was created with program beditimg specifying a cylinder centered at
461 75,75,45 with radius 20 and height 90, and a soft edge with a gaussian width of 3 pixels. The
462 softness of this mask was tuned to avoid high frequency correlations in the comparison of vertex
463 volumes. To address the symmetry mismatch between the fivefold vertex and the twelvefold
464 portal, the best 5-fold orientations of the portal-bearing vertices were found and refined
465 (program bico). The coordinates corresponding to the portal vertices were then transferred to
466 the parameter file referencing the full capsid volumes (program bico). Finally, the average of the
467 whole capsids was calculated with the portal vertex located at the top of the volume. Graphics
468 were prepared using PyMOL (52) and UCSF Chimera (53).
469
470 **<u>Data Availability:</u>**

471 Maps for the UL25-Null A-capsid and the procapsid, both showing the portal vertex, were
472 deposited in the Electron Microscopy Database under accession numbers EMDB-22378 and
473 EMDB-22379, respectively.
474

475 **Acknowledgements**

476 We thank Dr. Fred L. Homa (University of Pittsburgh) for providing us with the HSV-1 UL25-Null
477 mutants and the complementary, UL25-expressing African Green Monkey cell line as well as a
478 wild type African Green Monkey cell line. We thank Dr. Jay Brown for useful discussions. This
479 work was supported by the Intramural Research Program of the National Institute for Arthritis,
480 Musculoskeletal and Skin Diseases, NIH and used the NIH Multi-Institute CryoEM Facility (MICEF).
481

482 **Competing Interests:**

483 The authors declare no competing interests.
484

485 **References:**

486

487 1. Mettenleiter TC, Klupp BG, Granzow H. 2009. Herpesvirus assembly: an update. Virus
488 Res 143:222-34.
489 2. Newcomb WW, Homa FL, Thomsen DR, Booy FP, Trus BL, Steven AC, Spencer JV, Brown
490 JC. 1996. Assembly of the herpes simplex virus capsid: characterization of intermediates
491 observed during cell-free capsid formation. Journal of Molecular Biology 263:432-46.
492 3. Newcomb WW, Homa FL, Thomsen DR, Trus BL, Cheng N, Steven A, Booy F, Brown JC.
493 1999. Assembly of the herpes simplex virus procapsid from purified components and
494 identification of small complexes containing the major capsid and scaffolding proteins.
495 Journal of Virology 73:4239-50.
496 4. Newcomb WW, Trus BL, Cheng N, Steven AC, Sheaffer AK, Tenney DJ, Weller SK, Brown
497 JC. 2000. Isolation of herpes simplex virus procapsids from cells infected with a
498 protease-deficient mutant virus. Journal of Virology 74:1663-73.
499 5. Aksyuk AA, Newcomb WW, Cheng N, Winkler DC, Fontana J, Heymann JB, Steven AC.
500 2015. Subassemblies and asymmetry in assembly of herpes simplex virus procapsid.
501 mBio 6:e01525-15.
502 6. Huet A, Makhov AM, Huffman JB, Vos M, Homa FL, Conway JF. 2016. Extensive subunit
503 contacts underpin herpesvirus capsid stability and interior-to-exterior allostery. Nat
504 Struct Mol Biol 23:531-9.
505 7. Trus BL, Booy FP, Newcomb WW, Brown JC, Homa FL, Thomsen DR, Steven AC. 1996.
506 The herpes simplex virus procapsid: structure, conformational changes upon

507 maturation, and roles of the triplex proteins VP19c and VP23 in assembly. J Mol Biol
508 263:447-62.
509 8. Heymann JB, Cheng N, Newcomb WW, Trus BL, Brown JC, Steven AC. 2003. Dynamics of
510 herpes simplex virus capsid maturation visualized by time-lapse cryo-electron
511 microscopy. Nat Struct Biol 10:334-41.
512 9. Booy FP, Trus BL, Newcomb WW, Brown JC, Conway JF, Steven AC. 1994. Finding a
513 needle in a haystack: detection of a small protein (the 12-kDa VP26) in a large complex
514 (the 200-MDa capsid of herpes simplex virus). Proceedings of the National Academy of
515 Sciences, USA 91:5652-6.
516 10. Trus BL, Homa FL, Booy FP, Newcomb WW, Thomsen DR, Cheng N, Brown JC, Steven AC.
517 1995. Herpes simplex virus capsids assembled in insect cells infected with recombinant
518 baculoviruses: structural authenticity and localization of VP26. Journal of Virology
519 69:7362-6.
520 11. Bauer DW, Huffman JB, Homa FL, Evilevitch A. 2013. Herpes virus genome, the pressure
521 is on. J Am Chem Soc 135:11216-21.
522 12. Johnson DC, Baines JD. 2011. Herpesviruses remodel host membranes for virus egress.
523 Nat Rev Microbiol 9:382-94.
524 13. Mettenleiter TC, Muller F, Granzow H, Klupp BG. 2013. The way out: what we know and
525 do not know about herpesvirus nuclear egress. Cell Microbiol 15:170-8.
526 14. Heming JD, Conway JF, Homa FL. 2017. Herpesvirus Capsid Assembly and DNA
527 Packaging. Adv Anat Embryol Cell Biol 223:119-142.
528 15. Trus BL, Cheng N, Newcomb WW, Homa FL, Brown JC, Steven AC. 2004. Structure and
529 polymorphism of the UL6 portal protein of herpes simplex virus type 1. J Virol 78:12668-
530 71.
531 16. Newcomb WW, Thomsen DR, Homa FL, Brown JC. 2003. Assembly of the herpes simplex
532 virus capsid: identification of soluble scaffold-portal complexes and their role in
533 formation of portal-containing capsids. J Virol 77:9862-71.
534 17. Trus BL, Newcomb WW, Cheng N, Cardone G, Marekov L, Homa FL, Brown JC, Steven
535 AC. 2007. Allosteric signaling and a nuclear exit strategy: binding of UL25/UL17
536 heterodimers to DNA-Filled HSV-1 capsids. Mol Cell 26:479-89.
537 18. McElwee M, Vijayakrishnan S, Rixon F, Bhella D. 2018. Structure of the herpes simplex
538 virus portal-vertex. PLoS Biol 16:e2006191.
539 19. Liu YT, Jiang J, Bohannon KP, Dai X, Gant Luxton GW, Hui WH, Bi GQ, Smith GA, Zhou ZH.
540 2017. A pUL25 dimer interfaces the pseudorabies virus capsid and tegument. J Gen Virol
541 98:2837-2849.
542 20. Heming JD, Huffman JB, Jones LM, Homa FL. 2014. Isolation and characterization of the
543 herpes simplex virus 1 terminase complex. J Virol 88:225-36.
544 21. al-Kobaisi MF, Rixon FJ, McDougall I, Preston VG. 1991. The herpes simplex virus UL33
545 gene product is required for the assembly of full capsids. Virology 180:380-8.
546 22. Baines JD, Poon AP, Rovnak J, Roizman B. 1994. The herpes simplex virus 1 UL15 gene
547 encodes two proteins and is required for cleavage of genomic viral DNA. J Virol 68:8118-
548 24.

549 23. Yu D, Weller SK. 1998. Herpes simplex virus type 1 cleavage and packaging proteins
550 UL15 and UL28 are associated with B but not C capsids during packaging. J Virol
551 72:7428-39.
552 24. Adelman K, Salmon B, Baines JD. 2001. Herpes simplex virus DNA packaging sequences
553 adopt novel structures that are specifically recognized by a component of the cleavage
554 and packaging machinery. Proc Natl Acad Sci U S A 98:3086-91.
555 25. Sheaffer AK, Newcomb WW, Gao M, Yu D, Weller SK, Brown JC, Tenney DJ. 2001. Herpes
556 simplex virus DNA cleavage and packaging proteins associate with the procapsid prior to
557 its maturation. J Virol 75:687-98.
558 26. White CA, Stow ND, Patel AH, Hughes M, Preston VG. 2003. Herpes simplex virus type 1
559 portal protein UL6 interacts with the putative terminase subunits UL15 and UL28. J Virol
560 77:6351-8.
561 27. Newcomb WW, Juhas RM, Thomsen DR, Homa FL, Burch AD, Weller SK, Brown JC. 2001.
562 The UL6 gene product forms the portal for entry of DNA into the herpes simplex virus
563 capsid. J Virol 75:10923-32.
564 28. Cardone G, Winkler DC, Trus BL, Cheng N, Heuser JE, Newcomb WW, Brown JC, Steven
565 AC. 2007. Visualization of the herpes simplex virus portal in situ by cryo-electron
566 tomography. Virology 361:426-34.
567 29. Chang JT, Schmid MF, Rixon FJ, Chiu W. 2007. Electron cryotomography reveals the
568 portal in the herpesvirus capsid. J Virol 81:2065-8.
569 30. Rochat RH, Liu X, Murata K, Nagayama K, Rixon FJ, Chiu W. 2011. Seeing the portal in
570 herpes simplex virus type 1 B capsids. J Virol 85:1871-4.
571 31. Huet A, Huffman JB, Conway JF, Homa FL. 2020. The role of the herpes simplex virus
572 CVSC proteins at the capsid portal vertex. J Virol doi:10.1128/JVI.01534-20.
573 32. Liu YT, Jih J, Dai X, Bi GQ, Zhou ZH. 2019. Cryo-EM structures of herpes simplex virus
574 type 1 portal vertex and packaged genome. Nature 570:257-261.
575 33. Wang N, Chen W, Zhu L, Zhu D, Feng R, Wang J, Zhu B, Zhang X, Chen X, Liu X, Yan R, Ni
576 D, Zhou GG, Liu H, Rao Z, Wang X. 2020. Structures of the portal vertex reveal essential
577 protein-protein interactions for Herpesvirus assembly and maturation. Protein Cell
578 11:366-373.
579 34. Gong D, Dai X, Jih J, Liu YT, Bi GQ, Sun R, Zhou ZH. 2019. DNA-Packing Portal and Capsid-
580 Associated Tegument Complexes in the Tumor Herpesvirus KSHV. Cell 178:1329-1343
581 e12.
582 35. Gao M, Matusick-Kumar L, Hurlburt W, DiTusa SF, Newcomb WW, Brown JC, McCann PJ,
583 3rd, Deckman I, Colonno RJ. 1994. The protease of herpes simplex virus type 1 is
584 essential for functional capsid formation and viral growth. J Virol 68:3702-12.
585 36. McNab AR, Desai P, Person S, Roof LL, Thomsen DR, Newcomb WW, Brown JC, Homa FL.
586 1998. The product of the herpes simplex virus type 1 UL25 gene is required for
587 encapsidation but not for cleavage of replicated viral DNA. Journal of Virology 72:1060-
588 70.
589 37. Heymann JB. 2018. Guidelines for using Bsoft for high resolution reconstruction and
590 validation of biomolecular structures from electron micrographs. Protein Sci 27:159-171.
591 38. Dai X, Zhou ZH. 2018. Structure of the herpes simplex virus 1 capsid with associated
592 tegument protein complexes. Science 360.

593 39. Church GA, Dasgupta A, Wilson DW. 1998. Herpes simplex virus DNA packaging without
594 measurable DNA synthesis. J Virol 72:2745-51.
595 40. Machon C, Fabrega-Ferrer M, Zhou D, Cuervo A, Carrascosa JL, Stuart DI, Coll M. 2019.
596 Atomic structure of the Epstein-Barr virus portal. Nat Commun 10:3891.
597 41. Yang K, Baines JD. 2009. Tryptophan residues in the portal protein of herpes simplex
598 virus 1 critical to the interaction with scaffold proteins and incorporation of the portal
599 into capsids. J Virol 83:11726-33.
600 42. Dedeo CL, Cingolani G, Teschke CM. 2019. Portal Protein: The Orchestrator of Capsid
601 Assembly for the dsDNA Tailed Bacteriophages and Herpesviruses. Annu Rev Virol
602 6:141-160.
603 43. Singer GP, Newcomb WW, Thomsen DR, Homa FL, Brown JC. 2005. Identification of a
604 region in the herpes simplex virus scaffolding protein required for interaction with the
605 portal. J Virol 79:132-9.
606 44. Yang K, Baines JD. 2009. Proline and tyrosine residues in scaffold proteins of herpes
607 simplex virus 1 critical to the interaction with portal protein and its incorporation into
608 capsids. J Virol 83:8076-81.
609 45. Hong Z, Beaudet-Miller M, Durkin J, Zhang R, Kwong AD. 1996. Identification of a
610 minimal hydrophobic domain in the herpes simplex virus type 1 scaffolding protein
611 which is required for interaction with the major capsid protein. J Virol 70:533-40.
612 46. Guasch A, Pous J, Ibarra B, Gomis-Ruth FX, Valpuesta JM, Sousa N, Carrascosa JL, Coll M.
613 2002. Detailed architecture of a DNA translocating machine: the high-resolution
614 structure of the bacteriophage phi29 connector particle. J Mol Biol 315:663-76.
615 47. Thomsen DR, Newcomb WW, Brown JC, Homa FL. 1995. Assembly of the herpes simplex
616 virus capsid: requirement for the carboxyl-terminal twenty-five amino acids of the
617 proteins encoded by the UL26 and UL26.5 genes. J Virol 69:3690-703.
618 48. Pelletier A, Do F, Brisebois JJ, Lagace L, Cordingley MG. 1997. Self-association of herpes
619 simplex virus type 1 ICP35 is via coiled-coil interactions and promotes stable interaction
620 with the major capsid protein. J Virol 71:5197-208.
621 49. Draganova EB, Zhang J, Zhou ZH, Heldwein EE. 2020. Structural basis for capsid
622 recruitment and coat formation during HSV-1 nuclear egress. Elife 9.
623 50. Mastronarde DN. 2005. Automated electron microscope tomography using robust
624 prediction of specimen movements. J Struct Biol 152:36-51.
625 51. Heymann JB. 2021. High resolution electron tomography and segmentation-by-
626 modeling interpretation in Bsoft. Protein Science 30:44-59.
627 52. Schrodinger L. 2015. The PyMOL Molecular Graphics System, Version 18:1.
628 53. Pettersen EF, Goddard TD, Huang CC, Couch GS, Greenblatt DM, Meng EC, Ferrin TE.
629 2004. UCSF Chimera--a visualization system for exploratory research and analysis. J
630 Comput Chem 25:1605-12.
631
632

633 # Supplementary material

634

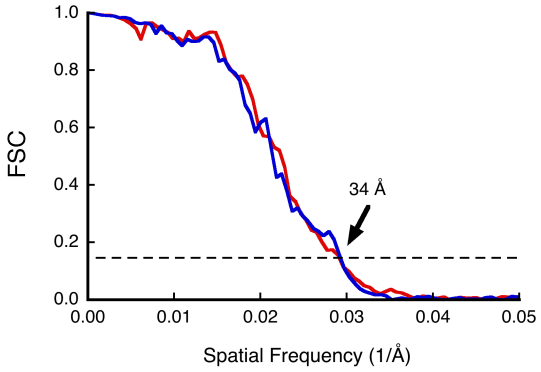

635

636 **Fig. S1.** Fourier shell correlation of subtomogram half-set averages of procapsids (red) and A-
637 capsids (blue) with the resolution indicated at a threshold of 0.143 (dashed line). A soft mask
638 covering the capsid shell and portal vertex was used in the analysis.

639